

Interfacial domain formation during magnetization reversal in exchange biased CoO/Co bilayers

F. Radu* , M. Etzkorn, R. Siebrecht, T. Schmitte, K. Westerholt, H. Zabel
Institut für Experimentalphysik/Festkörperphysik, Ruhr-Universität Bochum, 44780 Bochum, Germany

We have carried out detailed experimental studies of the exchange bias effect of a series of CoO/Co(111) textured bilayers with different Co layer thickness, using the magneto-optical Kerr effect, SQUID magnetometry, polarized neutron reflectivity, x-ray diffraction, and atomic force microscopy. All samples exhibit a pronounced asymmetry of the magnetic hysteresis at the first magnetization reversal as compared to the second reversal. Polarized neutron reflectivity measurements show that the first reversal occurs via nucleation and domain wall motion, while the second reversal is characterized by magnetization rotation. Off-specular diffuse spin-flip scattering indicates the existence of interfacial magnetic domains. All samples feature a small positive exchange bias just below the blocking temperature, followed by a dominating negative exchange bias field with decreasing temperature.

PACS numbers: 75.60.Jk, 75.70.Cn, 61.12.Ha

I. INTRODUCTION

The exchange bias phenomenon is associated with the interfacial exchange coupling between ferromagnetic and antiferromagnetic spin structures, resulting in an unidirectional magnetic anisotropy that causes a shift of the hysteresis loop to negative field values as one cools the system through the Néel temperature of the antiferromagnet(AF) in a positive magnetic field [1]. The exchange bias effect is essential for the development of magneto-electronic switching devices (spin-valves) and for random access magnetic storage units. For these applications a predictable, robust, and tunable exchange bias effect is required.

Extensive data have been collected on the exchange bias field H_{EB} , and the coercivity field H_c , for a large number of bilayer systems, which are reviewed in Ref. [2, 3]. The details of the EB effect depend crucially on the AF/F combination chosen and on the structure and thickness of the films. However, some characteristic features apply to most systems: (1) H_{EB} and H_c increase as the system is cooled in an applied magnetic field below the blocking temperature $T_B \leq T_N$ of the AF layer, where T_N is the Néel temperature of the AF layer; (2) the magnetization reversal can be different for the ascending and descending part of the hysteresis loop [4], as was first pointed out in reference [5], and recently also observed by Lee et al. [6] and Gierlings et al. [7]; (3) thermal relaxation effects of H_{EB} and H_c indicate that a stable magnetic state is reached only at very low temperatures [8, 9, 10]. Furthermore, a positive H_{EB} has been observed after cooling an AF/F system in very high magnetic fields [11, 12], and a perpendicular exchange bias was realized by using a ferromagnetic layer with perpen-

dicular anisotropy [13]. Several theoretical models have been developed for describing possible mechanisms of the EB effect, including domain formation in the AF layer with domain walls perpendicular to the AF/F interface [14], creation of uncompensated excess AF spins at the interface [15], or the formation of a domain wall in the AF layer parallel to the interface [19, 20]. Another approach is the consideration of diluted antiferromagnets in a field. In the work of Miltényi et al., Keller et al. [16, 17], and Nowak et al.[18] the discussion about compensated versus uncompensated interfacial spins is replaced by a discussion of net magnetic moments within the antiferromagnetic layer[21]. They show that perpendicular magnetic domain walls in the AF layer can effectively be pinned at defect sites, providing an enhanced exchange bias field. Recent overviews of theoretical models on the exchange bias effect are provided by Stamps [22] and by Kiwi [23]. However, so far there is still not a satisfactory agreement between the different theoretical approaches and experimental observations of the macroscopic and microscopic response of exchange bias systems.

One step forward in describing the exchange field behavior, as we will demonstrate in the present report, could come from a detailed analysis and understanding of the asymmetric behavior of the magnetization reversal and relaxation processes of the magnetization close to the coercive fields. To this end, we have chosen to investigate the archetypal CoO/Co(111) AF/F exchange bias system because it offers a number of advantages over similar systems, which show also the EB effect. First, Co has very good growth properties as a thin film and very flat interfaces can be prepared by sputtering and molecular beam epitaxial techniques. Second, the Néel temperature of the oxide is at a convenient temperature of 291 K. Third, CoO provides a large EB even for very thin layers, which can easily be prepared by thermal oxidation [24]. Furthermore, CoO/Co bilayers exhibit straightforward and pronounced EB properties, which qualifies them as a model system for detailed investigations of the magnetization reversal process [7, 17, 24, 25]. This is the

*Permanent address: Department of Experimental Physics, National Institute of Physics and Nuclear Engineering, P. O. BOX MG-6, 76900, Magurele, Romania.

case although the spin structure of the antiferromagnetic CoO is rather complex. In CoO the spin-orbit interaction and therefore the crystal anisotropy is strong. For bulk CoO the easy axis is reported to be along the [117] directions [26]. However, in very thin layers because of missing neighbors the easy axis has still to be determined. Training effects, which have been observed for CoO/Co, add an additional difficulty. However, training effects can also be useful for the understanding of the metastability of interfaces, as we will show further below.

In the present paper we investigate the thickness dependence of the exchange bias effect by using a wedge type CoO/Co(111) bilayer with a Co thickness varying from 27 Å to 400 Å. Previous studies by Gruyters and Riegel [24] have shown that the shape of the hysteresis changes dramatically with the Co thickness, indicating that aside from film orientation and exchange coupling the film thickness plays an important role for the type of domains formed and magnetization reversal observed. Here we report extensive hysteresis measurements of CoO/Co(111) bilayers, including a detailed analysis of the interfacial domain state by investigating the specular and off-specular neutron spin flip cross section at the coercive fields for descending and ascending magnetic fields.

II. SAMPLE PREPARATION AND CHARACTERIZATION

A series of nine samples were prepared by rf-sputtering in 99.99% Ar (samples s1-s9 in Table. I). The a-plane $\text{Al}_2\text{O}_3(11\bar{2}0)$ substrates were kept at 300° C during the Co deposition, which is the optimized growth temperature as concerns mosaicity, structural coherence length, and surface morphology, as determined in Ref. [27]. The substrate for sample s9 was placed in the middle of the sample holder while the other 8 substrates were placed at equal distances away from each other. Taking advan-

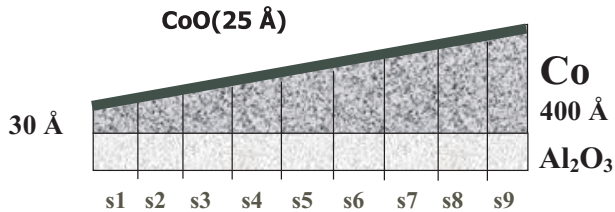


FIG. 1: The design of the wedge type CoO/Co(111) sample grown on a sapphire substrate. Before growth, the Al_2O_3 substrate is cut in 9 pieces and placed on the sample holder at equal distances away from each other. The gradient growth rate provides samples s1 to s9 of different thickness.

tage of the natural gradient in the sputtering rate, the samples acquire an increasing thickness from 30 Å (s1) to 400 Å (s9) (see Fig. 1). Subsequently, the samples were exposed to air at room temperature which results in

a 25 Å thick CoO layer on top of the Co film. The characterization of the surface morphology by Atomic Force Microscopy (AFM) shows an exceptionally low roughness of 1 Å for all samples, which has also been confirmed by x-ray reflectivity measurements performed at the W1.1 beam-line of the HASYLAB. As a representative example in Fig. 2 the reflectivity is shown for the thickest sample (s9) together with a best fit to the data points. The thickness parameters obtained for all samples from the fits are listed in Table I. High angle x-ray diffraction measurements (Fig. 2) show that the Co layer consists mainly of the cubic fcc phase with the (111) growth direction yielding a strong peak at $Q = 3.08 \text{ \AA}^{-1}$, and a minority hcp phase with a tilted $(10\bar{1}1)$ growth responsible for the peak at $Q = 3.25 \text{ \AA}^{-1}$. The observed 'fcc' peak position is closer to the ideal fcc position at $Q = 3.071 \text{ \AA}^{-1}$ than to the ideal hcp position at $Q = 3.106 \text{ \AA}^{-1}$, which is in good agreement with earlier measurements of Co films on sapphire substrates grown at the same substrate temperature and similar thicknesses[27]. The full width at half maximum (FWHM) of the rocking curve of the pseudo Co(111) Bragg peak is 0.01 degrees for an incoming wavelength of 1.393 Å, confirming a very good texture of the Co film. Natural oxidation of the Co(111) films leads to a preferential growth of CoO with (111) orientation. We have studied, in addition, epitaxial Co(111) layers, which have been thermally oxidized *in-situ*. Synchrotron diffraction studies of the in-plane CoO structure showed that [111] is the surface normal of the 2.5 nm thick CoO film [28]. By analogy we assume that for the highly textured CoO/Co bilayer used for the present study, the same orientational relationship holds. If the interface were ideal, this orientation would provide uncompensated spins and therefore would exhibit an exchange bias effect. This has been proven in the work of Gökemeijer et al.[29], who showed that for CoO/Co single crystalline films an exchange bias occurs only in the (111) orientation but not in the (110) and (100) orientations. The presence of uncompensated spins at the interface is one of the key requirements for achieving a shift of the hysteresis loop [16, 17, 18, 29], other important factors are AF exchange constant and AF magneto-crystalline anisotropy [14, 22].

We first show magnetic characterizations of the Co films in the unbiased state at room temperature by taking hysteresis loops with the magneto-optical Kerr effect (MOKE). Several hysteresis loops were taken with the field parallel to the film plane but with different azimuth angles of the sample. A plot of the ratio between the remanent magnetization and saturation magnetization M_{re}/M_{sat} , versus the rotation angle ϕ , reveals a two-fold in-plane anisotropy, which is observed for all samples and which is induced by the sapphire substrate. In addition a small contribution from a four-fold anisotropy can be recognized by closer inspection. These results are in complete agreement with earlier hysteresis measurements of Co(111) films on $\text{Al}_2\text{O}_3(11\bar{2}0)$ substrates [30]. A typical example for an unbiased hysteresis loop recorded at 270 K is plotted in Fig. 4 for sample s4. It is characterized by

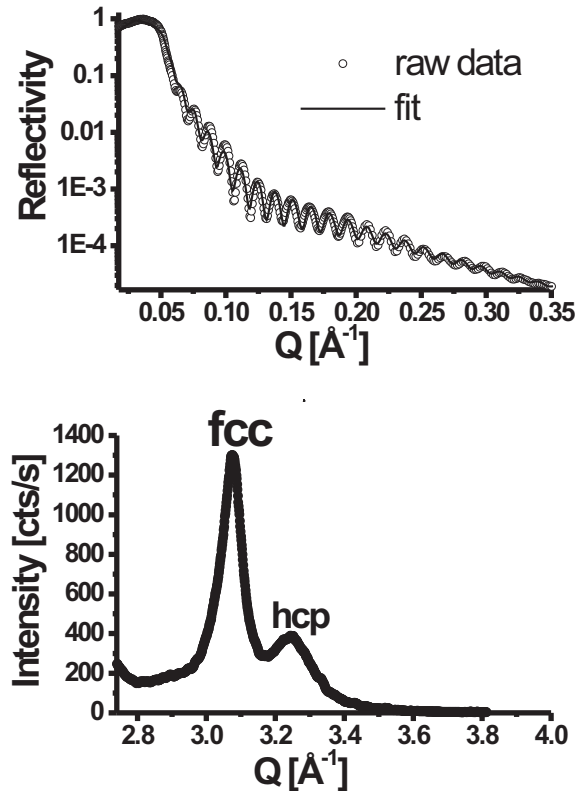


FIG. 2: Top panel: Reflectivity measurement of sample s9 (CoO(25Å)/Co(400Å)) using synchrotron radiation (open dots). The solid line shows a best fit to the data points. Bottom panel: X-ray radial Bragg scan parallel to the surface normal of CoO(25Å)/Co(150Å). The main peak at $Q = 3.08 \text{ \AA}^{-1}$ is close to the ideal fcc Co(111) position, indicating a majority fcc phase. The second peak is from a minority tilted hcp component with $[10\bar{1}1]$ orientation. The inset shows a transverse scan through the Co(111) peak.

a completely symmetric shape and a small coercive field of 60 Oe. Additional temperature dependent studies of the coercive field showed that the Néel temperature of a 25 Å thick CoO layer is about the same as in the bulk ($T_N = 291 \text{ K}$). In fact, it might even be slightly higher than in the bulk as shown in Ref.[31].

III. TEMPERATURE DEPENDENCE OF THE EXCHANGE BIAS AND COERCIVE FIELDS

The temperature dependence of the hysteresis loops for samples s1-s9 was measured by a superconducting quantum interference device (SQUID) magnetometer. The exchange bias field H_{EB} , the coercive fields H_{c1} and H_{c2} , and the half width of the total coercive field $H_c = |(H_{c1} - H_{c2})/2|$ were extracted from the hysteresis loops measured at temperatures between 310 and 5 K. The samples were cooled from above the Néel tempera-

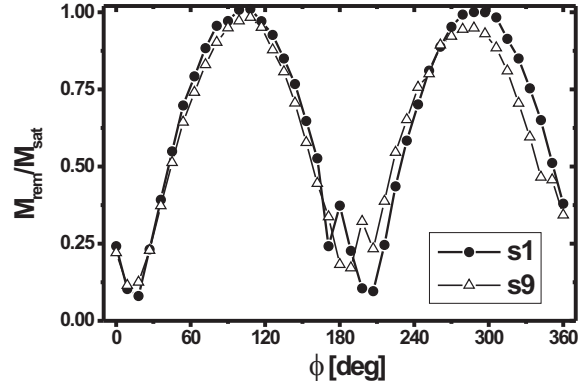


FIG. 3: Remanent magnetization divided by the saturation magnetization versus the rotation angle of the sample CoO(25Å)/Co(26 Å) (full circles) and CoO(25Å)/Co(400 Å) (open triangles) showing. The two fold anisotropy was observed for all samples.

ture to below different target temperatures in a magnetic field of $H_{FC} = +2000 \text{ Oe}$ applied closely along the easy axis of the sample magnetization. The procedure was repeated for each target temperature. In Fig. 4 typical hysteresis loops are shown for the sample s4 with a Co thickness of 87 Å and for the target temperatures 270 K, 160 K, 80 K, and 5 K. The hysteresis curves were taken directly after cooling and thus before training, unless otherwise stated. The hysteresis loops show the following typical and general features: H_{c1} increases strongly with decreasing temperature, while H_{c2} remains almost constant at a field value of about 300 Oe. The slope of the hysteresis loops at H_{c1} is steeper than at H_{c2} on the return path.

Fig. 5 summarizes the analysis of the temperature dependence of H_{c1} , H_{c2} , H_c , and H_{EB} for the samples s2 and s3. The top panel reproduces the coercive field of the first reversal H_{c1} and of the second reversal H_{c2} for the samples s3. Both coercive fields start to slightly increase just below the Néel temperature with the same rate of 0.21 Oe/K.

At the blocking temperature of about $T_B \approx 186 \text{ K}$, the slope increases drastically. Below T_B a bifurcation for the temperature dependence of H_{c1} and H_{c2} develops. While H_{c1} keeps rising with a rate of 11.1 Oe/K, H_{c2} levels off and reaches saturation at the lowest temperature. Thus, there are three distinguishable temperature regions: (1) from T_N to T_B the coercive fields are equal and increase slowly; (2) close to T_B the slopes increase drastically and H_{c1} is slightly smaller than H_{c2} ; (3) below T_B both coercive fields develop linearly but with different slopes such that the absolute value of H_{c1} is bigger than H_{c2} . Only in this last region a strong negative EB is observed. The different temperature dependencies of both coercive fields are consistent with the different magnetization reversal

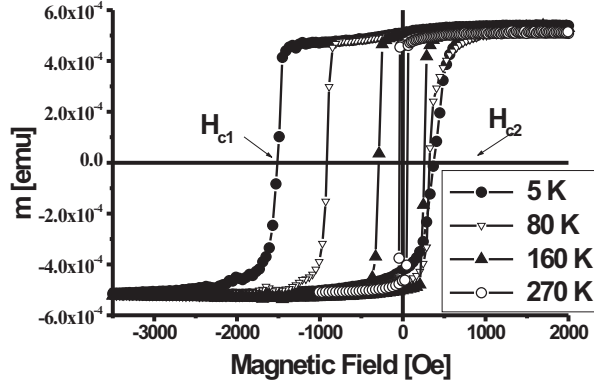


FIG. 4: Hysteresis loops for different temperatures of sample s4 (CoO(25Å)/Co(120Å)). For each hysteresis the bilayer was cooled in a field of +2000 Oe from 320K to the respective temperature. The hysteresis curves were taken after cooling and before training.

processes, which are recognized via polarized neutron reflectivity measurements at these points to be discussed further below. Previous studies of CoO/Co thin film systems have shown an inverse proportionality between the exchange bias field and the Co layer thickness [24]. Our experiments completely confirm these results and extend the linearity down to a thickness of 27 Å (see Table. I and Fig. 7).

In Fig. 5 the exchange bias and coercive fields for samples s2 and s3 are shown. At $T_B=186$ K the H_{EB} becomes positive and reaches a maximum of $H_{EB} = +20$ Oe. The temperature region of the positive EB is shown on an enlarged scale in the inset of Fig. 5. This surprising feature has been observed for all our samples. After changing sign, H_{EB} decreases steadily as the temperature is lowered. Because of the sign change we define the blocking temperature T_B as the temperature where H_{EB} first deviates from zero. This definition coincides with a linear extrapolation of H_{c1} to zero, shown by the solid line in the bottom panel.

The linear dependence of H_c and H_{EB} on the temperature is in good agreement with reports from other CoO/Co bilayers [17, 24, 33]. A positive H_{EB} close to T_B is seen in our bilayers for the first time [34]. Positive exchange bias fields have been reported in the literature, but only for high cooling fields, when the external field exceeds the interfacial coupling, breaking the parallel alignment between the F and AF layer [11, 12]. Recently, three further papers have reported about the observation of a positive exchange bias effect [35, 36, 37]. In contrast to those papers we observe a weakening of the positive exchange bias after training. This is shown in Fig. 6.

The positive exchange bias is considered as a proof for an antiparallel alignment of the spins at the AF/F interface in moderate cooling fields [11]. For parallel align-

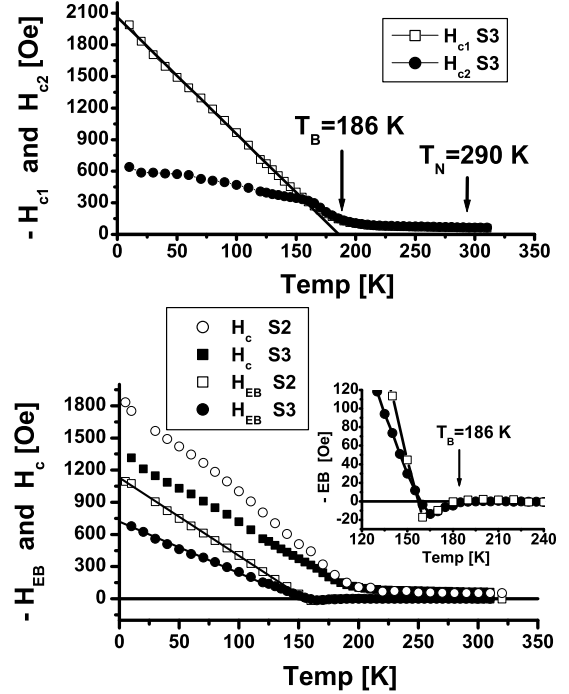


FIG. 5: Top panel: Coercive fields H_{c1} and H_{c2} of sample s3. The line is a fit to the linear region of H_{c2} . It intersects the abscissa at the blocking temperature $T_B = 186$ K. Bottom panel: temperature dependence of the coercive field and the exchange bias field for samples s2 and s3. In the inset the positive exchange bias occurring close to the blocking temperature is shown. The lines are guides to the eye.

ment of the magnetic moments in the F and AF layers the bias field would not change sign even in high fields. Therefore, the change of sign from negative to positive exchange bias as a function of applied field hints to antiferromagnet interfacial coupling requiring a superexchange mechanism working at the F/AF interface[38].

In order get more insight into the origin of the positive exchange bias, we have measured its field cooling dependence shown in Fig. 8. The sample s2(see Table. I) was cooled down from $T=320$ K to 175 K in different applied fields, ranging from -20 Oe to 40 kOe (see the inset of (Fig. 8)). First observation is that the exchange bias is positive for all cooling fields. Second the bias field is constant and about +20 Oe between 1 kOe and 40 kOe, but below 1 kOe the bias field increases dramatically to twice its former value. This increase is solely due to a shift of H_{c1} to smaller values with decreasing cooling field, while H_{c2} remains constant. We also note that the increasing EB field correlates with a decreasing remanence at 320 K as the cooling field is lowered. Thus for small cooling fields the initial magnetic state of the sample is not fully saturated. At these small cooling fields (< 1000 Oe) we

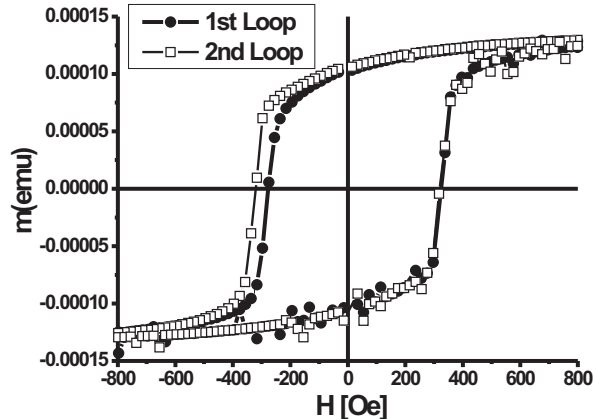


FIG. 6: First (solid circles) and second hysteresis (open squares) loop taken at 175 K. For the second hysteresis loop H_{c1} decreased while H_{c2} remained constant, implying a reduction of the positive exchange bias after training.

observe a surprisingly strong increase of the EB field.

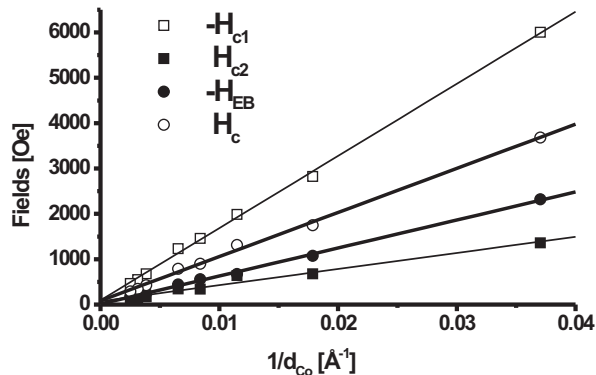


FIG. 7: $-H_{c1}$ (open squares), H_{c2} (full squares), $-H_{EB}$ (full circles), H_c (open circles) are plotted as a function of the Co thickness. The samples were cooled down through the Néel temperature of CoO to 10 K in an applied magnetic field of +2000 Oe. The lines are linear fits to the data points.

This behavior can be explained assuming two contributions to the interfacial exchange coupling. Normally the interface exchange coupling is ferromagnetic between CoO and Co as already mentioned above, being the result of a direct exchange of Co monolayers on either side of the ferro- and antiferromagnetic layer[38]. For a positive exchange bias effect we have to assume that some parts at the interface are, however, antiparallel coupled. Then, an antiparallel alignment may be caused by a superexchange type of mechanism mediated by an oxygen monolayer at the interface. It is reasonable to assume that due to roughness or thickness fluctuations, small fractions of the CoO film may be oxygen terminated instead of metal

terminated at the interface.

Next we discuss the training effect in the region below the blocking temperature [4, 25], which is different from the training for the positive exchange bias Fig.6. After closing a complete loop the hysteresis becomes symmetric and assumes an S-like shape. The H_{c1} field for all subsequent loops and the EB-field is smaller than for the first reversal. Thus the trained hysteresis has a different shape and a smaller EB field than the hysteresis of the virgin sample. Obviously the first reversal is dominated by a different process than the following reversals, transforming the sample from a unique and irreversible state to a different state with reproducible and symmetric branches of the descending and ascending parts of the hysteresis

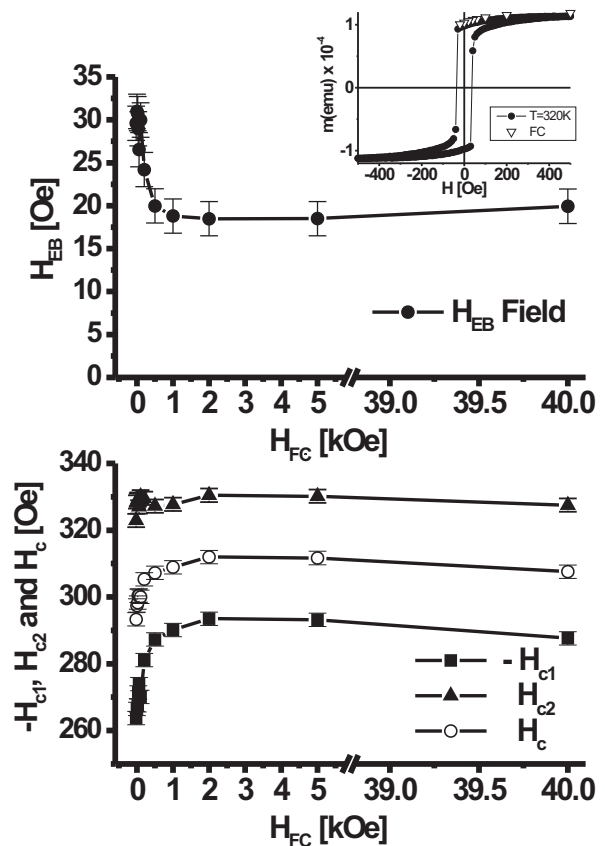


FIG. 8: Top: The field cooling dependence of the positive exchange bias for sample s2 (CoO(25Å)/Co(56Å)). The bilayer was cooled in different fields from above the Néel temperature of CoO to 175 K, where hysteresis loops were measured. The inset shows a hysteresis loop at $T=320$ K (full dots), together with the cooling field values (down triangles) as reference of the initial state of the sample. Bottom: The dependence of the coercive field values ($-H_{c1}$, H_{c2} and $H_c = (-H_{c1} + H_{c2})/2$) as a function of the applied cooling field. The lines are guides to the eyes.

loop. When the sample is first cooled in a positive field, the Co layer consists of a single ferromagnetic domain. Upon cooling below the blocking temperature, the orien-

tation of antiferromagnetic domains in CoO is affected by the exchange coupling at the AF/F interface. To optimize the interfacial energy and to avoid spin frustration it is favorable for the CoO film to develop a multi-domain

TABLE I: Values for in-plane coercive and exchange bias fields and for Co layer thicknesses of a wedge type Co/CoO sample are listed. The thickness of the CoO layer is constant and about 25 Å. The coercive fields H_{c1} and H_{c2} and the exchange bias field H_{EB} are for samples which were cooled in a field of 2000 Oe from above the Néel temperature(290 K) to 10 K.

Sample index	d_{Co} [Å]	H_{c1} [Oe]	H_{c2} [Oe]	H_{EB} [Oe]	H_c
s1	27	-6004	1362	-2321	3683
s2	56	-2825	677	-1073	1751
s3	87	-1990	640	-675	1315
s4	119	-1458	343	-557	901
s5	153	-1233	346	-443	789
s7	260	-678	176	-251	427
s8	320	-549	144	-202	346
s9	398	-464	115	-174	290

state. However, after cooling in the saturation field of the ferromagnetic layer, the frustrated spins at the interface may very well be preserved, which would yield a CoO layer in a single domain state. The lower the interface roughness, the higher will be the probability for a single domain state. The first reversal at H_{c1} changes the magnetic state of the interface, leaving behind a more disordered spin structure. A more precise analysis of the processes which occur at the CoO/Co interface is possible with polarized neutron reflectivity measurements, to be discussed next.

IV. POLARIZED NEUTRON REFLECTOMETRY

In order to gain more insight into the reversal mechanism in decreasing and increasing magnetic fields, we have performed polarized neutron reflectivity (PNR) measurements on Co/CoO bilayers, using the angle dispersive neutron reflectometer ADAM at the Institut Laue-Langevin, Grenoble [39] with a fixed wavelength of 4.41 Å. Preliminary results are presented in Ref. [4]. The sample has been optimized for the needs of neutron reflectivity and consists of a CoO(25Å)/Co(200Å) bilayer grown under the same conditions as explained above, but on a Ti(2000 Å)/Cu(1000 Å)/Al₂O₃ neutron resonator template. This configuration of the sample allows to observe with high sensitivity the ferromagnetic domains and the spin misalignment at the interfaces[40, 41, 42].

The method we used to study the magnetization reversal by PNR includes the following concepts: (1) the dependence of spin asymmetry measured at one specific value of the wave vector transfer depends only on the cosine of the angle (θ) between the magnetic induction in the magnetic layer and the neutron polarization direction; (b) the spin-flip reflectivity is proportional to

$\sin^2(\theta)$; (c) the off-specular scattering shows the existence of magnetic domains within the magnetic layer; (d) the enhancement of the neutron density achieved at the magnetic interface, using the neutron resonator, increases the off-specular scattering from the interfacial magnetic domain walls.

In order to find the optimized scattering vectors for measuring neutron hysteresis loops, we have first recorded a complete set of polarized neutron reflectivities for all four cross-sections. The raw data without experimental corrections (spin flip efficiency and footprint) is shown in Fig. 9. The measurements were carried out at room temperature and close to the coercive field. Since at room temperature without exchange bias, reversal is dominated by coherent rotation, the resonant peaks in the spin-flip reflectivities are strong and well defined. We used this information to choose the proper wavevector ($Q_{SF}=0.016 \text{ \AA}^{-1}$) for recording the spin-flip intensity as a function of the applied magnetic field at low temperatures. Similar, for the non-spin flip intensities we have fixed the scattering vector just above the critical edge for total external reflection of the unpolarized beam ($Q_{NSF}=0.019 \text{ \AA}^{-1}$). SF and NSF refer to spin flip and non-spin flip scattering, respectively. We have chosen this Q_{NSF} value, because it provides the highest contrast for non-spin flip reflectivity from the magnetic layer combined with high intensity, whereas Q_{SF} provides the maximum intensity.

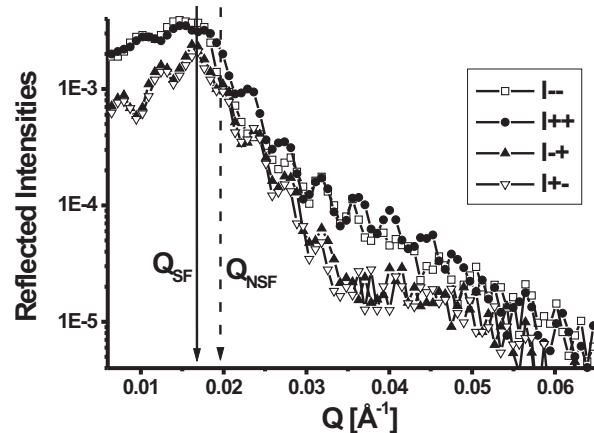


FIG. 9: Polarized neutron reflectivity measurements of a CoO/Co/Ti/Cu/Al₂O₃ resonator sample taken at room temperature in a magnetic field of about 60 Oe ($=H_{c1}$). The arrows for Q_{NSF} and Q_{SF} denote the points where non-spin flip and spin flip intensities were recorded at low temperature after field cooling.

The magnetic hysteresis loop can be measured by PNR using the Spin Asymmetry (SA) defined as:

$$SA(k_z, \theta, \mathbf{B}) = \frac{R^+ - R^-}{R^+ + R^-} = \frac{R^{++} - R^{--}}{R^{++} + R^{+-} + R^{-+} + R^{--}}, \quad (1)$$

where R^{++} , R^{+-} , R^{-+} , and R^{--} are the four reflectivities from a magnetic multilayer system, $R^+ = R^{++} + R^{+-}$, $R^- = R^{--} + R^{-+}$, and θ is the angle between the neutron polarization axis and the direction of the magnetic induction $\mathbf{B} = \mathbf{H} + 4\pi\mathbf{M}$, with \mathbf{M} being the magnetization of the ferromagnetic layer. k_z is the perpendicular component of the incoming wave vector. The spin asymmetry, depends obviously on the optical parameters and the thickness of the layers. They have been omitted in the variable list because they are constant.

For a single magnetic layer embedded in a non-magnetic matrix the SA is expressed as:

$$SA(k_z, \theta, \mathbf{B}) = SA(k_z, 0, |\mathbf{B}|)\cos(\theta) \approx B_x/|\mathbf{B}|, \quad (2)$$

where $B_x = |\mathbf{B}|\cos(\theta)$ is the component of the magnetic induction parallel to the polarization axes. For a simple case we derive this expression in the appendix.

The spin-flip reflectivities are:

$$R^{\pm\mp} \approx \sin(\theta)^2 \approx B_y^2/|\mathbf{B}|^2, \quad (3)$$

where $B_y = |\mathbf{B}|\sin(\theta)$ is the perpendicular (to the neutron polarization direction) component of the magnetic induction.

The equations 2 and 3 are directly related to the perpendicular and parallel components of the magnetic induction of a ferromagnetic layer. Moreover, through the spin flip scattering one can decide whether the magnetization reversal is dominated by rotation or domain wall movement.

The magnetic hysteresis ($SA(Q_{NSF}, \theta, \mathbf{B})/SA(Q_{NSF}, 0, |\mathbf{B}_{\text{sat}}|) = SA/SA(0) = \cos(\theta) = B_x/|\mathbf{B}|$) loop measured by PNR is shown in Fig. 10 together with the magnetic hysteresis obtained by MOKE from the same sample. The field dependencies of the non-spin flip (NSF) reflectivities, from which the magnetic hysteresis is derived, are shown in panels (b) and (c). The non-spin flip reflectivities were measured at a wave vector transfer Q corresponding to the inflection point of the non-polarized neutron reflectivity (near the critical edge for total external reflection) and by sweeping the magnetic field in the usual manner. Note that for technical reasons the MOKE hysteresis curve was taken at 50 K while the neutron measurements were performed at 10 K. Both curves show the same asymmetric shape at H_{c1} and H_{c2} as discussed before. The different H_{c1} values for the MOKE and PNR measurements are solely due to the different sample temperatures. Nonetheless, we find very good agreement between both loops during the first reversal. On the return path through H_{c2} the agreement is by far not as good as one would expect if no specular intensity loss were occurring due to off-specular diffuse scattering.

On the other hand, this discrepancy between MOKE and PNR is an indication for the presence of magnetic domains in the ferromagnetic layer on the return path. This will be discussed in more detail in the appendix (section IV.2).

In addition to the standard magnetization curves, PNR is capable of distinguishing between different magnetization reversal processes and to provide information on magnetic domains by analyzing the specular and the off-specular spin flip (SF) intensities I^{+-} and I^{-+} . Specular SF scattering is sensitive to magnetization components in the sample plane, which are perpendicular to the applied field direction. The off-specular SF signal reveals the presence of magnetic domains [43].

We first discuss the specular spin flip intensities shown by triangles in panels (b) and (c) of Fig. 10. They were measured at the scattering vector Q corresponding to the resonance peak near the critical edge. The magnetization reversal at H_{c2} exhibits strong spin-flip intensities I^{+-} and I^{-+} . This is always observed for rounded or 'trained' hysteresis loops and is characteristic for a magnetization reversal via domain rotation [44]. Magnetization reversal by rotation provides a large magnetization component perpendicular to the field or polarization axis, giving rise to neutron spin-flip process. Vice versa, the rather low spin-flip intensities, which are observed during the first magnetization reversal in the virgin state at H_{c1} are indicative of pure 180° domain wall movement. The step like intensity change at $H_{c1} = -750$ Oe is followed by a steady decrease as the system approaches saturation (see Fig. 10e). The slightly enhanced specular spin-flip scattering takes place in a very narrow field range of not more than 15 Oe [FWHM=9 Oe]. From these features it is obvious that domain wall nucleation and propagation let the magnetic spins at the interface canted away from the applied field direction.

Next we discuss the off-specular spin flip scattering close to H_{c1} , which is reproduced in Fig. 10d. The off-specular diffuse intensities taken at $H_{c1} = -750$ Oe, at $H = -1400$ Oe, and upon return to $H = -230$ Oe are rather strong. Their asymmetric shape is attributed to the specific wave-vector where they have been measured[45]. Note that the off-specular intensity appears only after the magnetization reversal at H_{c1} has taken place for the first time and is negligible before. The solid line in Fig. 10d is the SF scattering taking in a descending field at -530 Oe (before first magnetization reversal), representing the instrumental resolution. After reversal the diffuse scattering is large, then decreases towards saturation in negative fields and increases again on the way back towards H_{c2} . The diffuse spin flip scattering reveals the existence of magnetic domains walls[45]. We argue that those domain walls are located at the interface between the ferromagnetic and antiferromagnetic layer and that they have to be distinguished from ferromagnetic domains in the Co layer. If the diffuse scattering were originating from domain walls inside of the Co-layer, then the off-specular scattering should vanish in saturation, which

is clearly not the case here. The creation of interfacial domains is crucial for the change of the reversal character from domain wall motion at H_{c1} to domain rotation at H_{c2} . The breakdown of the ferromagnetic film in domains along the trained hysteresis has also been observed by Velthuis et al. [25]. Here we show that the breakdown occurs already during the very first reversal and does not heal anymore even in saturation. Opposite to Velthuis et al. [25] we argue that the observed domain formation is the reason for the trained hysteresis curve, instead of training being the cause for a partial breakdown of the alignment of the ferromagnetic domains.

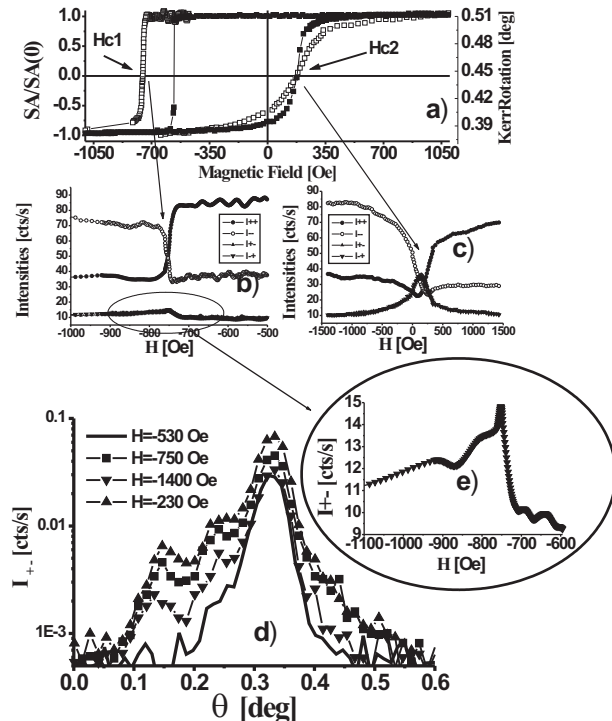


FIG. 10: (a) MOKE hysteresis loop (full squares) and neutron hysteresis loop (open squares) of a CoO/Co bilayer after field cooling to 50K (MOKE) and to 10 K (neutrons) in an external field of +2000 Oe. (b) and (c) The specular non spin-flip intensities I_{++} and I_{--} and the specular spin-flip intensities I_{+-} and I_{-+} are plotted as a function of external magnetic field. The intensities are measured at special scattering vector values of the reflectivity curves (see text); (d) Off-specular diffuse spin-flip scattering taken before magnetization reversal at -530 Oe (line), at $H_{c1} = -750$ Oe (full squares), in saturation at -1400 Oe (down full triangles) and before the second magnetization reversal at -230 Oe (up full triangles); (e) A zoom in from panel d) showing the I_{+-} intensity at the first magnetization reversal.

The PNR results lead us to the following interpretation of the magnetization reversal in an EB-field. At H_{c1} the magnetization reversal takes place via nucleation and

domain wall movement and leaves the interface in a (partial) magnetic domain state. The spins in the interfacial domains are strongly coupled to the antiferromagnet and even in saturation they are not aligned along the external field direction. Those interface spins give rise to the strong off-specular diffuse spin-flip scattering. Upon returning from saturation in negative fields we notice an increase of the diffuse spin flip scattering, which suggests that a torque is acting on the ferromagnetic spins trying to reverse them back to the direction of the cooling field long before the magnetization reversal actually takes place. It seems that those interfacial magnetic domains are the seeds of the second magnetization reversal at H_{c2} , which proceeds via domain rotation. The domain rotation at H_{c2} is characterized by a large specular spin-flip scattering (panel c of Fig. 10) and off-specular diffuse scattering (not shown). Therefore the second and all other reversals are dominated by domain rotation processes.

The behavior of the interface layer as revealed by PNR is in good qualitative agreement with the observation of uncompensated spins at the CoO/Co interface by Gruyters and Riegel [24] and with the model put forward by Mauri and co-workers [19]. The latter authors suggest the formation of a domain wall parallel to the interface during reversal of the FM orientation, which can effectively lower the interfacial energy cost of reversing the FM layer without removing the condition of strong interfacial AF/F coupling. The interface may be considered as a diluted antiferromagnet. This should be distinguished from the work of Miltenyi et al. [17], who purposely keep the defects away from the interface. It would be desirable to image the interfacial domains by real space methods such as done recently via polarized electron emission microscopy [47]. This methods can, however, only be applied in remanence. Ferromagnetic domains as they develop at the interface and in high fields can presently only be followed via polarized neutron reflectivity.

V. CONCLUSIONS

In summary, using a wedge type sample with a Co thickness gradient we have determined the coercive fields and the exchange bias field after field cooling for different Co layer thicknesses. The exchange bias field at low temperature follows the $1/d_{FM}$ behavior. In addition, the temperature dependence of the exchange bias field exhibits a small positive value just below the blocking temperature, which is most likely due to a superexchange mechanism with antiferromagnetic exchange coupling at the AF/F interface. With polarized neutron reflectivity measurements we have shown that the first magnetization reversal at H_{c1} is dominated by nucleation and domain wall motion, while the second magnetization reversal at H_{c2} can be described by magnetization rotation. All subsequent reversals are similar to the second,

yielding a symmetric hysteresis, which, however, remains shifted. Furthermore diffuse spin-flip scattering reveals the formation of magnetic domains at the interface, induced by the first magnetization reversal. We have shown that these magnetic domains are preserved even in saturation and that they serve as seeds for the second magnetization reversal. Overall, our data reveal clear differences between the coercive fields of the very first reversal H_{c1} and the second reversal at H_{c2} . The mechanisms of the magnetization reversal (domain wall motion versus domain rotation) and their temperature dependencies are clearly distinct.

VI. APPENDIX

For the sake of clarity we shall demonstrate the formulae 2 and 3 for a simple case. Let us consider a semi-infinite magnetic media for which we shall obtain the analytical formulae of reflectivities. We start from the general formalism presented in Ref. [40]. Using the expression $\hat{\boldsymbol{\mu}} = \mu \hat{\boldsymbol{\sigma}}$ and the well known properties of the Pauli operator ($\hat{\boldsymbol{\sigma}}$) one can write the expression of the wave vector operator as:

$$\hat{k}_i^+ = \frac{k_i^+ + k_i^-}{2} + (\hat{\boldsymbol{\sigma}} \mathbf{e}_i) \frac{k_i^+ - k_i^-}{2},$$

where $k_i^\pm = \sqrt{k_z^2 - u_i \mp |\boldsymbol{\mu} \mathbf{B}_i| \frac{2m}{\hbar^2}}$ are the eigenvalues of the operator \hat{k}_i^+ and $\mathbf{e}_i = \mathbf{B}_i/B_i$ is a unit vector which defines the direction of the magnetic induction in the i^{th} media, $u_i = 4\pi N_i b_i^{coh}$ is the nuclear scattering length density of the i -the layer, where N is the nuclear density and b^{coh} is the coherent scattering length. The matrix representation of $\hat{R}_i = \hat{\boldsymbol{\sigma}} \mathbf{e}_i$ reads:

$$R = \begin{pmatrix} \cos(\theta) & \sin(\theta)e^{-i\phi} \\ \sin(\theta)e^{i\phi} & -\cos(\theta) \end{pmatrix},$$

where θ and ϕ are the polar and the axial angle in the spherical coordinates with the polar axis being the quantization axis. Choosing the quantization axis to be parallel to the polarization axis, the matrix representation of the reflection operator $\hat{\rho}_{01}$ becomes:

$$\rho_{01} = \begin{pmatrix} r^{++} & r^{-+} \\ r^{+-} & r^{--} \end{pmatrix}$$

$$r^{++} = \frac{k_1^- k_0^+ - 2 k_1^- k_1^+ + k_0^+ k_1^+ - k_0^- (k_1^- - 2 k_0^+ + k_1^+) + (k_0^- + k_0^+) (k_1^- - k_1^+) \cos(\theta)}{k_1^- k_0^+ + 2 k_1^- k_1^+ + k_0^+ k_1^+ + k_0^- (k_1^- + 2 k_0^+ + k_1^+) - (k_0^- - k_0^+) (k_1^- - k_1^+) \cos(\theta)} \quad (4)$$

$$r^{--} = -\frac{k_1^- k_0^+ + 2 k_1^- k_1^+ + k_0^+ k_1^+ - k_0^- (k_1^- + 2 k_0^+ + k_1^+) + (k_0^- + k_0^+) (k_1^- - k_1^+) \cos(\theta)}{k_1^- k_0^+ + 2 k_1^- k_1^+ + k_0^+ k_1^+ + k_0^- (k_1^- + 2 k_0^+ + k_1^+) - (k_0^- - k_0^+) (k_1^- - k_1^+) \cos(\theta)} \quad (5)$$

$$r^{+-} = \frac{2 k_0^+ (k_1^- - k_1^+) e^{i\phi} \sin(\theta)}{k_1^- k_0^+ + 2 k_1^- k_1^+ + k_0^+ k_1^+ + k_0^- (k_1^- + 2 k_0^+ + k_1^+) - (k_0^- - k_0^+) (k_1^- - k_1^+) \cos(\theta)} \quad (6)$$

$$r^{-+} = \frac{2 k_0^- (k_1^- - k_1^+) e^{-i\phi} \sin(\theta)}{k_1^- k_0^+ + 2 k_1^- k_1^+ + k_0^+ k_1^+ + k_0^- (k_1^- + 2 k_0^+ + k_1^+) - (k_0^- - k_0^+) (k_1^- - k_1^+) \cos(\theta)} \quad (7)$$

It is easy to check that the expressions above are the same as ones obtained by Pleshanov [50].

In order to understand how the reflectivities depend on the magnetization reversal in an ferromagnetic media let us consider the case when $k_z = u$. Choosing just a single value for the incident wave vector and sweeping

the applied magnetic field is a key ingredient for measuring a complete hysteresis loop via PNR. We neglect the neutron absorption into the sample and consider the case when the applied magnetic field is much smaller then the internal fields into the ferromagnetic media. With these assumptions and for $B_x \geq 0$ the reflectivities become:

$$R^{++} = |r^{++}|^2 = \frac{1 + V_{mn}^2 + 2\sqrt{V_{mn}} (1 + V_{mn}) \cos(\theta) + 2 V_{mn} \cos(\theta)^2}{(1 + \sqrt{V_{mn}})^2 (1 + V_{mn})}$$

$$R^{--} = |r^{--}|^2 = \frac{1 + V_{mn}^2 - 2\sqrt{V_{mn}} (1 + V_{mn}) \cos(\theta) + 2 V_{mn} \cos(\theta)^2}{(1 + \sqrt{V_{mn}})^2 (1 + V_{mn})}$$

$$R^{+-} = R^{-+} = |r^{\pm\mp}|^2 = \frac{2 V_{mn} \sin(\theta)^2}{(1 + \sqrt{V_{mn}})^2 (1 + V_{mn})},$$

where $V_{mn} = Vm/V_n = |\mu B|/(\frac{\hbar^2}{2m} 4\pi N b_{coh})$ is the ra-

tio of the magnetic to the nuclear potential. The con-

clusion from the formulae above are that at the critical scattering vector for non-polarized neutron, the reflectivities:

- depend on the absolute value of the magnetization induction;
- depend on the relative orientation between the polarization axis and the direction of the magnetic induction into the media;
- do not depend on the polar angle ϕ .

We consider below two cases: one when the magnetization reversal proceeds by rotation and another case where the magnetization changes through domain wall movement.

1. Coherent rotation of the magnetization

Let us consider that the magnetic moments will rotate during the magnetization reversal in such a way that $B = B_{sat}$ with the components $B_y = B \cos(\theta)$ and $B_x = B \sin(\theta)$. The easiest way to imagine such a rotation is to rotate the sample instead of rotating the magnetic moment, keeping the remanent magnetization equal to the saturation magnetization ($M_{rem}/M_{sat} = 1$). With this assumption the spin asymmetry $SA(k_z, \theta, |\mathbf{B}|)$ becomes:

$$SA(k_z, \theta, \mathbf{B}) = (R^+ - R^-)/(R^+ + R^-) = \frac{2\sqrt{V_{mn}} \cos(\theta)}{1 + V_{mn}} = \frac{B_x}{|\mathbf{B}|} \frac{2\sqrt{V_{mn}}}{1 + V_{mn}}$$

$$SA(k_z, \theta, \mathbf{B}) = SA(k_z, 0, |\mathbf{B}|) \frac{B_x}{|\mathbf{B}|}$$

The spin flip reflectivity is:

$$R^{+-} = \frac{2V_{mn} \sin(\theta)^2}{(1 + \sqrt{V_{mn}})^2 (1 + V_{mn})} = B_y^2 \frac{1}{B_{sat}^2} \frac{2V_{mn}}{(1 + \sqrt{V_{mn}})^2 (1 + V_{mn})}$$

$$R^{+-} = B_y^2 f(B_{sat}, V_{mn})$$

Measurements of R^+ and R^- at any k_z value as a function of the applied magnetic field provide the same hysteresis loop as obtained by MOKE or SQUID measurements. Moreover, fitting the non-spin flip reflectivity curves taken in saturation (R^+ or R^- or both) one can accurately evaluate the absolute magnetic moment. In comparison, for MOKE one would have to make a calibration for the Kerr angles and for SQUID one needs to determine the volume of the magnetic layer.

where a magnetic film consists of ferromagnetic domains with the following configuration: a fraction of n domains have their spins oriented parallel to the neutron polarization and a fraction of $1 - n$ domains have the spin oriented antiparallel. The measured reflectivities would not be simply R^+ or R^- but given by $I^+ = nR^+ + (1 - n)R^-$ and $I^- = (1 - n)R^+ + nR^-$. The measured spin asymmetry becomes:

2. Domain Wall Movement

Now we discuss a magnetization reversal by domain wall movement. For simplicity we consider a situation

$$SA(k_z, \theta, |\mathbf{B}|) = \frac{I^+ - I^-}{I^+ + I^-} = (2n - 1) \left(\frac{R^+ - R^-}{R^+ + R^-} \right) = B_x \frac{1}{B_{sat}} \frac{\sqrt{V_{mn}}}{1 + V_{mn}},$$

where $B_x = (2n - 1)|\mathbf{B}|$ with $|\mathbf{B}|$ being the magnetic induction into the magnetic domains. Thus, the shape of the hysteresis loop is completely defined. The spin flip scattering will result only from domain walls.

In a more general case when for instance the magnetic domains are rotated with respect to the neutron polarization axis, there will also be spin flip scattering. For

this case the SA expression will still be valid and, in addition, from the spin-flip scattering their angle relative to the neutron polarization axis can be measured.

We mention that the formulae above are only correct in the absence of off-specular scattering. The values of SA and the spin-flip reflectivity will be affected by the loss of the specular signal. This can be seen when comparing

SQUID or MOKE based magnetic hysteresis loops to the one extracted from the SA. Regions where the loops do not overlap indicate the presence of magnetic domains. This can be clearly seen in Fig. 10(a).

A different approach for evaluating the average magnetization vectors inside of a film in a domain state was taken by Lee et al. [6]. Instead of measuring the magnetization reversal at one specific wave vector, complete reflectivity curves are recorded and the average magnetization as well as the mean square dispersion of the domains as function of k_z is evaluated. They use similar reflectivity formulae as shown above, but do not derive magnetization loops. For a quantitative comparison of hysteresis loops the method presented here is faster and

more effective.

Acknowledgments

We gratefully acknowledge support through the Sonderforschungsbereiche 491 "Magnetische Heteroschichten: Struktur und elektronischer Transport" of the Deutsche Forschungsgemeinschaft. The neutron scattering experiments were performed at the ADAM reflectometer of the ILL, which is supported by the BMBF grant No. 03ZAE8BO. Special thanks are to Erik A. Verduijn for critical reading of the manuscript.

-
- [1] W. Meiklejohn and C. P. Bean, Phys. Rev. **102**, 1413 (1956) ; **105**, 904 (1957).
- [2] A. E. Berkowitz, K. Takano, J. Magn. Magn. Mater., **200**, 552-570 (1999).
- [3] J. Nogues, I. K. Schuller, J. Magn. Magn. Mater., **192**, 203-232 (1999).
- [4] F. Radu, M. Etzkorn, T. Schmitte, R. Siebrecht, A. Schreyer, K. Westerholt, H. Zabel, J. Magn. Magn. Mater., **240**, 251 (2002).
- [5] M. R. Fitzsimmons, P. Yashar, C. Leighton, Ivan K. Schuller, J. Nogues, C. F. Majkrzak and J. A. Dura, Phys. Rev. Lett. **84**, 3986 (2000).
- [6] W.-T. Lee, S. G. E. te Velthuis, G. P. Felcher, F. Klose, T. Gredig, and E. D. Dahlberg, Phys. Rev. B **65**, 224417 (2002).
- [7] M. Gierlings, M.J. Prandolini, H. Fritzsche, M. Gruyters, and D. Riegel, Phys. Rev. B **65**, 092407 (2002).
- [8] F. Radu, M. Etzkorn, V. Leiner, T. Schmitte, A. Schreyer, K. Westerholt, H. Zabel, Appl. Phys. A **74** Suppl1, S1570 (2002).
- [9] A. M. Goodman, H. Laidler, K. O'Grady, N. W. Owen, A. K. Petford-Long, J. Appl. Phys, **87**, 6409 (2000).
- [10] D. S. Geoghegan, P. G. McCormick, R. Street, J. Magn. Magn. Mater. **177**, 937 (1998).
- [11] J. Nogues, D. Lederman, T. J. Moran, and Ivan K. Schuller, Phys. Rev. Lett. **76**, 4624 (1996).
- [12] T. M. Hong, Phys. Rev. B **58**, 97 (1998).
- [13] S. Maat, K. Takano, S. S. P. Parkin, and Eric E. Fullerton, Phys. Rev. Lett., **87**, 087202-1 (2001).
- [14] A. P. Malozemoff, Phys. Rev. B **35**, 3679 (1987).
- [15] T.C. Schulthess and W.H. Butler, Phys. Rev. Lett. **81**, 4516 (1998).
- [16] J. Keller, P. Miltényi, B. Beschoten, G. Güntherodt, U. Nowak, and K. D. Usadel Phys. Rev. B **66**, 014431 (2002).
- [17] P. Miltényi, M. Gierlings, J. Keller, B. Beschoten, G. Güntherodt, U. Nowak, K. D. Usadel, Phys. Rev. Lett. **84**, 4224 (2000).
- [18] U. Nowak, K. D. Usadel, J. Keller, P. Miltényi, B. Beschoten, and G. Güntherodt Phys. Rev. B **66**, 014430 (2002).
- [19] D. Mauri, H. C. Siegmann, P. S. Bagus, and E. Kay, J. Appl. Phys., **62**, 3047 (1987).
- [20] M. D. Stiles, R. D. McMichael, Phys. Rev. B **59**, 3722 (1999).
- [21] A. Hoffmann, J. W. Seo, M. R. Fitzsimmons, H. Siegwart, J. Fompeyrine, J.-P. Locquet, J. A. Dura, and C. F. Majkrzak, Phys. Rev. B **66**, R220406 (2002).
- [22] R. L. Stamps, J. Phys. D:Appl. Phys. **33**, 247-268 (2000).
- [23] M. Kiwi, J. Magn. Magn. Mater. **234**, 584 (2001).
- [24] M. Gruyters and D. Riegel, Phys. Rev. B **63**, 052401 (2000).
- [25] S. G. E. te Velthuis, A. Berger, G. P. Felcher, B. K. Hill, E. Dan Dahlberg, J. Appl. Phys., **87** (2000) 5046.
- [26] W.L.Roth, Phys. Rev. **110**, 1333 (1958).
- [27] Ch. Morawe, A. Stierle, N. Metoki, K. Bröhl, and H. Zabel, J. Magn. Magn. Mater. **102**, 223 (1991).
- [28] F. Radu, K. Theis-Bröhl, M. Etzkorn, H. Zabel, to be published.
- [29] N. J. Gökemeijer, R. L. Penn, D. R. Veblen, C. L. Chien, Phys. Rev. B **63**, 174422 (2001).
- [30] N. Metoki, Th. Zeidler, A. Stierle, K. Bröhl, and H. Zabel, J. Magn. Magn. Mater. **118**, 57 (1993).
- [31] P. J. van der Zaag, Y. Ijiri, J. A. Borchers, L. F. Feiner, R. M. Wolf, J. M. Gaines, R. W. Erwin, and M. A. Verheijen, Phys. Rev. Lett., **84**, 6102 (2000).
- [32] M. R. Fitzsimmons, C. Leighton, A. Hoffmann, P. C. Yashar, J. Nogues, K. Liu, C. F. Majkrzak, J. A. Dura, H. Fritzsche, and I. K. Schuller, Phys. Rev. B **64**, 104415 (2001).
- [33] C. Schlenker, Phys. Status Solidi, **28**, 507 1968.
- [34] F. Radu, M. Etzkorn, T. Schmitte, V. Leiner, A. Schreyer, K. Westerholt, H. Zabel, Annual Report 2000, page 70 (http://www.ep4.ruhr-uni-bochum.de/fk/Publicationen/03_contribut).
- [35] T. Gredig, I. N. Krivorotov, P. Eames, D. Dahlberg, Appl. Phys. Lett. **81**, 1270 (2002).
- [36] T. L. Kirk, O. Hellwig, E. E. Fullerton, Phys. Rev. B **65**, 224426 (2002).
- [37] R. L. Compton, M. J. Pechan, S. Maat, E. E. Fullerton, Phys. Rev. B **66**, 054411 (2002).
- [38] F. T. Parker, Kentaro Takano, A. E. Berkowitz, Phys. Rev. B **61**, R866 (2000).
- [39] R. Siebrecht, A. Schreyer, U. Englisch, U. Pietsch and H. Zabel Physica B **241-243**, 169 (1998)
- [40] F. Radu, V. K. Ignatovich, Physica B **267**, 175 (1999) .
- [41] V. L. Aksenov, Yu. V. Nikitenko, F. Radu, Yu. M. Gledenov, P. V. Sedyshev, Physica B **276-278**, 946 (2000).
- [42] V. K. Ignatovich, F. Radu, Phys. Rev. B **64**,

- 205408(2001).
- [43] B.P. Toperverg, Physica B **297**, 160 (2001).
- [44] The *domain rotation* applies to the magnetization reversal process which shows both magnetic spin rotation revealed by neutron spin-flip scattering and presence of magnetic domains seen from spin-flip off-specular scattering.
- [45] F. Radu, A. Vorobiev, J. Major, H. Humblot, K. Westerholt, H. Zabel, arXiv:cond-mat/0212099 (2002), Physica B, *in print*, (2002).
- [46] B.N. Engel, C.D. England, R.A. Van Leeuwen, M.H. Wiedmann, D.M. Falco, Phys. Rev. Lett **67**, 1910 (1991).
- [47] H. Ohldag, T. J. Regan, J. Stör, F. Nolting, J. Lüning, C. Stamm, S. Anders, and R. L. White, Phys. Rev. Lett., **87**, 247201-1 (2001).
- [48] O. Hellwig, S. Maat, J. B. Kortright, and Eric E. Fullerton, Phys. Rev. B, **65**, 144418 (2002).
- [49] C. Leighton, M. R. Fitzsimmons, A. Hoffmann, J. Dura, C. F. Majkrzak, M. S. Lund, and Ivan K. Schuller, Phys. Rev. B **65**, 064403 (2002).
- [50] N. K. Pleshanov, Z. Phys. B **94**, 233 (1994).